Semiempirical (ZINDO-PCM) Approach to Predict the Radiative and Nonradiative Decay Rates of a Molecule Close to Metal Particles

Marco Caricato* and Oliviero Andreussi

Scuola Normale Superiore, piazza dei Cavalieri 7, 56126 Pisa, Italy

Stefano Corni

INFM-CNR National Research Center on nanoStructures and bioSystems at Surfaces (S³), v. Campi 213/A, 41100 Modena, Italy

Received: April 29, 2006; In Final Form: June 20, 2006

In this work, we present an extension of a model previously proposed (Andreussi et al. *J. Chem. Phys.* **2004**, *121*, 10190) to treat the effect of a metal particle on the optical properties of a molecule in solution (close to such a particle) in the framework of the polarizable continuum model (PCM). This extension concerns the combination of such a model with the semiempirical method Zerner's intermediate neglect of differential overlap (ZINDO), which allows us to treat large size molecular systems, as the ones normally used in the experiments. A refinement of the model is also introduced to take into account the effect of the metal specimen on the absorption process of the molecular system, which affects the probability that a molecule reaches the excited state. Numerical tests are presented to validate the reliability of the ZINDO results with respect to quantum-mechanical DFT methods. Comparisons with experimental results on two different large molecular systems are reported, and the effect of the metal on the absorption process is discussed.

1. Introduction

A molecule in an excited state can decay back to the ground state via radiative or nonradiative ways. When the molecule is placed close to a metal surface, the efficiency of both these decay channels can be affected. This phenomenon usually leads to the quenching of fluorescence (i.e., a decrease of the fluorescence quantum yield) and was experimentally verified a long time ago for planar metal surfaces.[1] For a molecule close to metal nanoparticles, experiments probing the radiative and nonradiative decay rates of the molecule at a known distance from the metal nanoparticle began to appear only recently.[2,3] From the theoretical point of view, different groups tackled the problem of calculating molecular lifetimes for systems close to a metal particle.[4−8] In particular, Gersten and Nitzan (GN)[4] considered a classical description of the metal particle, based on a local, frequency-dependent dielectric constant and limited their theory to analytically solvable shapes (spheroids and spheres as a special case). Ekardt and Penzar[7] considered instead a quantum-mechanical (QM) representation of the metal particle, based on the jellium model. Such an approach enlightens the quantum-size effects due to the electron confinement in the metal nanoparticle, deemed important for particle diameters smaller than 2−3 nm.[9] More recently, Leung[8] reconsidered the spherical Gersten−Nitzan model, introducing some effects of the nonlocality of the metal dielectric response via a hydrodynamic dielectric constant approach. All these methods share the same model of the molecule, treated as an oscillating point dipole. Some of us have recently proposed a model for the calculation of radiative and nonradiative lifetimes of excited molecules that goes well-beyond the point dipole approximation, whereas conserving computational feasibility.[10,11] In our model, the molecule is described at the QM level (HF and DFT in previous works), whereas the dielectric based description of the metal, common to the Gersten−Nitzan and Leung works, is used. However, differently from these authors, our implementation is based on a numerical approach that allows us to treat nanoparticles with complex shapes, not just spheres or ellipsoids (see ref 11 for some examples). In ref 11, we applied our method to a system that has been experimentally studied by Dulkeith et al.,[2] that is, lissamine anchored at a fixed distance to Au nanoparticles of variable radius. There, one of the typical dichotomies between theoretical and experimental studies appeared: optical experiments need complex dye molecules to match the experimental requirements (e.g., high optical efficiency, chemical stability, solubility, possibility to be chemically anchored to the nanoparticle) whereas high-level theoretical calculations, such as Kohn−Sham DFT, require instead small chromophores to keep the computational burden in an acceptable range. The solution that we adopted in that article was, as done often in these cases, to simplify the chromophore. One of the aims of the present article is to extend our model to a QM method able to treat molecular systems as large as usual dyes. Such a method is Zerner's intermediate neglect of differential overlap (ZINDO),[12] a semiempirical approach specifically parametrized to reproduce spectroscopic data. Among the QM methods cheaper than DFT, ZINDO appeared to us as the most suitable choice, thanks to this spectroscopy-oriented parametrization. With the ZINDO treatment of the molecule in hand (section 2.2), we shall reconsider our previous calculations on lissamine (section 3.1), showing that the choice of the model was indeed justified and did not contribute to the discrepancy with the experimental data. Then, the new method will be applied to another system recently studied by Dulkeith et al.,

* To whom correspondence should be addressed. E-mail: marco.caricato@yale.edu. Present address: Department of Chemistry, Yale University, 225 Prospect St., New Haven, CT 06520-8107.

10.1021/jp0626418 CCC: $33.50
Published on Web 07/29/2006

that is, Cy5 at variable distance from fixed radius Au nanoparticles.[3] Again, we shall take advantage of the newly implemented ZINDO procedure to treat the whole chromophore used in the experiment.

In the present article, we shall also deal with another refinement of our model for fluorescence. We already remarked that the presence of the metal directly affects the radiative and nonradiative molecular decay. However, when studying fluorescence of a molecule close to a metal specimen, one should not forget that the metal is also able to affect the *excitation* of the molecule from the ground state. If the excitation is done by irradiation (as in the vast majority of fluorescence experiments), then the metal can enhance or suppress the light absorption by the molecule and thus it can modify the probability that a molecule reaches the excited state. If the metal enhances the absorption, then the intensity of the fluorescence signal results enhanced as well, not withstanding the direct metal effects on the radiative decay rate. Some of the reports of enhanced fluorescence may arise from this effect.[13] Taking into account such an indirect effect on emission is also important when the aim is the study of the radiative lifetime of the molecule close to a metal specimen. In fact, as we shall discuss, radiative lifetimes can be related to the fluorescence intensity just after the excitation, which, however, also depends on the excited-state population. In the present work, we shall discuss how the metal effects on the absorption can be calculated in the framework of the model sketched above, and we shall quantify such effects for experimentally studied systems.

The article is organized as follows: A theoretical review of the model is presented in section 2. The correction to the experimental measurements to take into account the effect of a metal particle on the absorption process of a molecule is described in section 2.1, and the features of the combination of PCM with the semiempirical method ZINDO are treated in section 2.2. Section 3 concerns numerical applications to lissamine, section 3.1, and to Cy5, section 3.2. Finally, in section 4, some concluding remarks will be given.

2. Theoretical Background

To describe the interaction of a molecule with a metal particle, we have used the model recently proposed in refs 10 and 11. In this model, the molecule, which has the main role in the phenomenon under study, is described at a quantum-mechanical level whereas the metal (and the solvent, if present) is considered as a continuous body characterized by its response properties to electric fields, both the ones imposed on the system from outside and the ones arising from the molecular charge distribution.

The metal particle can have an arbitrary shape, obtained by a series of interlocking spheres.[11] It behaves as a perfect conductor in the presence of static fields, whereas its response to time-dependent electric fields is described through the experimental frequency-dependent permittivity, possibly modified to take into account quantum-size effects (especially the reduced mean free path of the metal electrons in nanoparticle).[10] The solvent is described as a continuum medium which hosts the solute in a cavity of proper shape and which fills all the free space. The metal−molecule and the solvent−molecule interactions have been described by using the PCM,[14] implemented in a local version of GAUSSIAN03.[15]

Here, we do not report all the methodological details, which the interested reader can find in refs 10 and 11, but we focus the attention on the quantities strictly related to the experimental data. In particular, the model allows us to compute the nonradiative and radiative decay rates, by using methods based on the linear response approximation (LRA).

As for the former property, it is related to the fact that the response of the metal at an optical frequency ω is described by a complex dielectric permittivity. The metal-induced nonradiative decay rate $\Gamma_{\mathrm{met}}^{\mathrm{nonrad}}$ can be associated with the imaginary part of the poles of the response function of the molecule that interacts with the metal.

On the other hand, the radiative decay rate Γ^{rad} is expressed as

$$\Gamma^{\mathrm{rad}} = \frac{4\omega^3 n_1}{3\hbar c^3} |\vec{\mu}_{\mathrm{K0}}|^2 \tag{1}$$

where ω is the fluorescence frequency corresponding to the transition under study (it corresponds to the real part of the pole of the response function), n_1 is the refractive index of the medium in which emission takes place, and $\vec{\mu}_{\mathrm{K0}}$ is the molecular transition dipole between the excited state K and the ground state. This transition dipole is the sum of two terms: $\vec{\mu}_{\mathrm{K0}}^{\mathrm{mol}}$, the transition dipole of the molecule in the complex environment, as computed in LRA, and $\vec{\tilde{\mu}}_{\mathrm{K0}}$, the dipole induced in the metal/solvent by the molecular transition, calculated as in ref 11.

We are mainly interested on the effect of the metal body on the response of the molecule and in comparing such an effect with the experimental findings. However, due to the intrinsic accuracy of the quantum-mechanical models that we are using, some discrepancies between theoretical and experimental results may be present independently of the presence of the metal. To single out the metal effect and taking into account that all the quantities we can calculate depend, to the first order, on $|\vec{\mu}_{\mathrm{K0}}^{\mathrm{mol}}|^2$, we scaled all the calculated results by the same ratio given by $f_0 = [\Gamma_0^{\mathrm{rad}}]_{\mathrm{exp}}/[\Gamma_0^{\mathrm{rad}}]_{\mathrm{calc}}$, where Γ_0^{rad} is the radiative decay rate for the molecule in solution without the metal. We verified that $|\vec{\mu}_{\mathrm{K0}}^{\mathrm{mol}}|^2$ is not particularly affected by the metal−molecule distance or by the particle radii, thus justifying the use of a single scaling factor. We also remark that a similar assumption has been used in ref 10, where the agreement with experimental results was quite satisfactory.

When comparing results for the nonradiative decay rate with the experiments, one has not to forget that molecules have intrinsic nonradiative decay rates that are present independently from the metal. We have taken these values from the experiments, and we assumed that they did not change in the presence of the metal (i.e., $\Gamma_0^{\mathrm{nonrad}} = [\Gamma_0^{\mathrm{nonrad}}]_{\mathrm{exp}}$). The final expression for Γ^{nonrad} is thus

$$\Gamma^{\mathrm{nonrad}} = \Gamma_{\mathrm{met}}^{\mathrm{nonrad}} + \Gamma_0^{\mathrm{nonrad}} \tag{2}$$

The relative magnitude of $\Gamma_{\mathrm{met}}^{\mathrm{nonrad}}$ and $\Gamma_0^{\mathrm{nonrad}}$ clearly depends on the studied system, especially on the metal−molecule distance. As we shall see in the numerical section, for typical dyes at nanometric distances, $\Gamma_{\mathrm{met}}^{\mathrm{nonrad}}$ prevails over $\Gamma_0^{\mathrm{nonrad}}$.

2.1. Absorption Correction. As pointed out in the Introduction, to compare our theoretical results with the experimental outcomes, a careful analysis of the reported quantities should be done: whereas the calculated quantities are strictly related only to the emission process, the experimental results may implicitly be related also to the absorption process. In fact, the radiative decay rate can be estimated by experimental data by means of the following expression[16]

$$\Gamma^{rad} = \Gamma_0^{rad} \frac{I_{fluo}^{met}(t=0)}{I_{fluo}^{0}(t=0)} \tag{3}$$

where $I_{fluo}^{met}(t=0)$ is the fluorescence light intensity just after excitation for the molecule close to the metal and $I_{fluo}^{0}(t=0)$ is the same quantity but without the metal. Equation 3 is strictly valid only when exactly the same number of molecules are promoted to the excited state by the incident radiation. If the absorption cross section is different with and without the metal, then a different number of excited molecules will be present at $t = 0$ and eq 3 does not apply. However, it is easy to see that a new equation can be written

$$\Gamma^{rad} = \Gamma_0^{rad} \frac{I_{fluo}^{met}(t=0)A^{0}}{I_{fluo}^{0}(t=0)A^{met}} \tag{4}$$

where $A^{0/met}$ is the absorption coefficient at the frequency of the light excitation. We remark that A^{met} is not the total absorption of the molecule + metal system but just the absorption due to the molecule close to the metal. Thus, an experimental determination of this quantity is not straightforward. For example, in refs 2 and 3, the Gersten−Nitzan model has been used to calculate the ratio A^0/A^{met} and to correct the bare experimental results. Similarly to the approach used to calculate Γ^{rad}, it is possible to quantitatively evaluate the effect of the metal on the absorption efficiency by exploiting our PCM-like model. In this case, the quantity of interest is given by

$$A = \frac{2\pi}{3\hbar^2 c n_1} |\vec{\mu}_{K0}|^2 \tag{5}$$

where, as for eq 1, the transition dipole is the sum of two terms, the one coming out from the LRA plus the one induced in the metal/solvent, but the response of the system is calculated at the absorption frequency. Since the response properties of the metal can vary substantially in this range of frequency, the transition dipole can be different from the emission one. Thus, for each metal−molecule configuration, calculations should be repeated at the absorption frequency. Note that we are not explicitly considering the Franck−Condon structure of the absorption band. However, since in eq 4 only the ratio A^0/A^{met} appears, not the single absorption coefficients, the Franck−Condon factors will mostly cancel out.

We remark that, in principle, also the experimental nonradiative decay rate depends on the correction for the differential absorption, since it is obtained as the total decay rate minus the radiative one.

2.2. ZINDO/PCM. In our previous works, the model described above for the metal has been combined with the time-dependent density functional theory (TDDFT) and time-dependent Hartree−Fock (TDHF) descriptions of the molecule. Although these QM levels of calculation are very accurate, they limit the size of the systems which can be treated. To apply this model to large molecules, as the ones generally used in experiments, in this paper we have extended the model to the semiempirical method ZINDO, recently combined with PCM.[17] Here, we briefly summarize the theory of ZINDO/PCM. In PCM, the electrostatic interactions between the molecule, hosted in a molecularly shaped cavity, and the surrounding environment are expressed in terms of *apparent surface charges* placed on the discretized boundaries of the different dielectric media that models such an environment (the solvent and the metal particle in the present case). In the Integral Equation Formalism version of PCM (IEFPCM),[18] these apparent charges **q** are obtained by solving a system of linear equations $\mathbf{Qq} = \mathbf{V}$ where the coefficients matrix **Q** is related to the dielectric constants and to the geometry of the boundaries, while **V** collects the electrostatic potential V_i produced by the molecule in the same position where the apparent charge q_i is placed.

The potential created by the charges **q** enters the resolutions of the self-consistent HF or DFT problem as described in previous articles.[14] The main difference in the application of PCM in a semiempirical framework, with respect to the ab initio framework, is in the definition of the electrostatic potential V_i. Using a semiempirical description, the electrostatic potential produced by the solute nuclear charges has a simple form

$$V_i^N = \sum_{\alpha}^{atoms} - \frac{Z'_\alpha}{|\mathbf{r}_\alpha - \mathbf{s}_i|} \tag{6}$$

where the nuclear charge Z'_α is reduced for the core electrons and the denominator is the distance modulus between the nucleus α and the position of the charge i, called $\mathbf{s}_i$. As for the potential produced by the solute electrons, $\hat{V}_i^E$, it is represented by a one-electron operator. In the INDO method, the one-electron integrals involving two different basis functions centered on the same atom and an operator centered on another atom are neglected. In the case of PCM, the operator $\hat{V}_i^E$ is centered in $\mathbf{s}_i$ (i.e., not on any atoms), therefore only the one-electron integrals involving the same basis functions μ_A centered on the same atom A are kept, $\langle\mu_A|\hat{V}_i^E|\mu_A\rangle$. These integrals are calculated through a multipole expansion of the elementary charge distribution $\mu_A^*\mu_A$.

For the evaluation of the excitation energy, the ZINDO approach[12] uses the Tamm−Dancoff approximation (TDA), also called configuration interaction singles (CIS).[19] This method is based on a monodeterminantal wave function as the reference state, and it can be seen as a specific case of the more general random phase approximation (RPA).

3. Numerical Applications

In this section, we show the results on lissamine and Cy5 molecules. The first system has been chosen to verify that the ZINDO method would provide reliable results, compared with the ones provided by TDDFT. In fact, we have tested ZINDO with systems already studied in a previous paper.[11] In that paper the nonradiative and the radiative decay rates, Γ_{met}^{nonrad} and Γ^{rad}, were computed as functions of the radius of the metal particle. These systems are shown in Figure 1 and are called antra and lissa. They represent simplified models of a larger system, called lissamine, used in an experiment reported in ref 2 (see Figure 1).

Since ZINDO has provided results in a good agreement with the TDDFT ones, we have performed the same calculations on the largest system, the lissamine, which was not treated in ref 11 because of its size.

In the second part of this section, the second system is studied, Cy5, shown in Figure 2. A recent experimental study[3] showed measurements of Γ^{nonrad} and Γ^{rad} on this molecule. In this case, instead of the particles size, the distance between the metal surface and the molecule is increased. Fluorescence quenching is experimentally reported for all the systems, decreasing with increasing dye−metal distance.

As even this molecule is quite large, we have studied it at the ZINDO level, assuming, also in this case, that it can provide results comparable with the TDDFT ones.

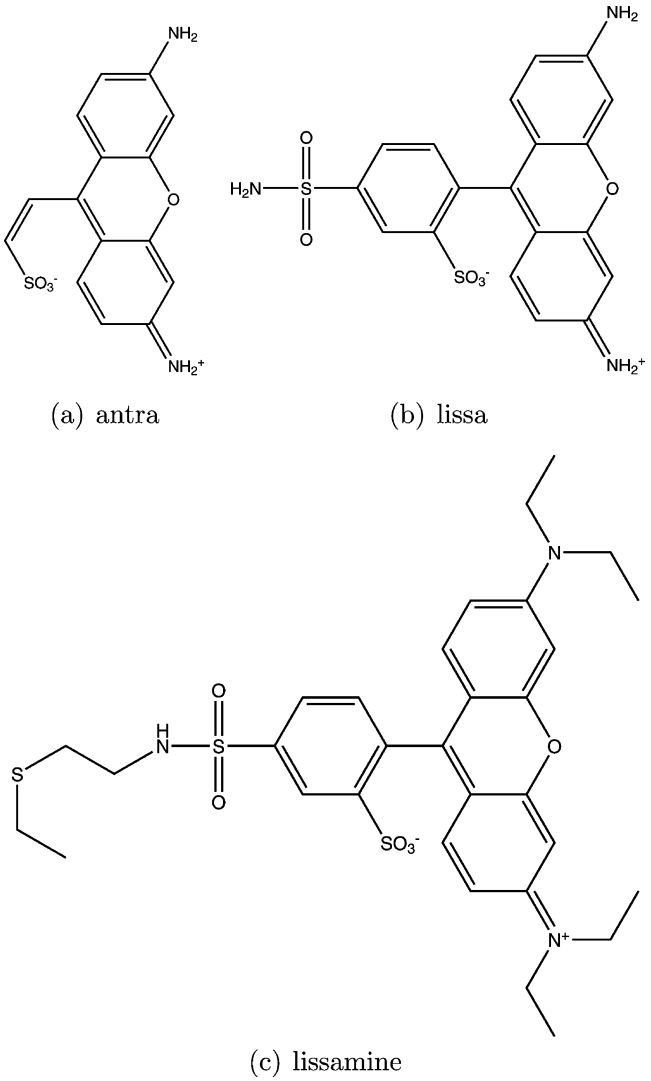

Figure 1. Structures of the systems antra (a), lissa (b), and lissamine (c).

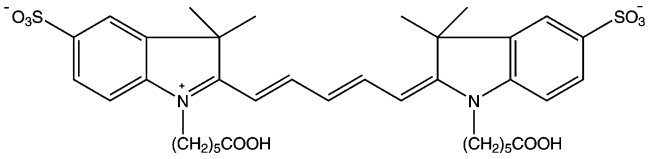

Figure 2. Structure of the Cy5 molecule.

3.1. Lissamine. The results presented in this section are divided into three parts. In the first part, the comparison between TDDFT and ZINDO methods are treated, showing how they perform on the small systems, antra and lissa. This allows us to test the ZINDO performance, even from a computational effort point of view. In the second part, only ZINDO results are shown, for the calculation on the simplified systems antra and lissa as well as on the whole lissamine molecule. In the last part, only the lissamine molecule at the ZINDO level is treated, analyzing the importance of taking into account the absorption process, described in section 2.1, for the agreement with experimental data.

3.1.1. Computational Details. Geometry optimizations have been performed at the AM1 and AM1-PCM levels, for the calculations in vacuo and in solution, respectively. We have used the same geometries for the calculations with TDDFT and ZINDO to produce comparable results. As for the systems antra and lissa, the calculations at the DFT level have been performed by using the B3LYP hybrid functional[20] with a 6-311+G(d) basis set. For all the calculations in solution, the PCM cavity is built as a series of interlocking spheres centered on atoms with radii:[21] 1.7 Å for C, 1.9 Å for CH, 2.0 Å for CH_n ($n = 2, 3$), 1.52 Å for O, 1.6 Å for N, 1.8 Å for S, and 1.2 Å for H not bonded to C, all multiplied by a cavity size factor of 1.2. The solvent, water, is represented by its static dielectric constant $\epsilon = 78.39$ and by its optical dielectric constant $\epsilon_\infty = 1.776$. For the metal, gold, the values of the dielectric constants at the different frequencies have been taken from the handbook by Palik:[22] for the emission process, at 595 nm, we have used $\mathrm{Re}\{\epsilon^{\mathrm{met}}\} = -8.831$ and $\mathrm{Im}\{\epsilon^{\mathrm{met}}\} = 1.329$; for the absorption process, at 400 nm, we have used $\mathrm{Re}\{\epsilon^{\mathrm{met}}\} = -1.0769$ and $\mathrm{Im}\{\epsilon^{\mathrm{met}}\} = 6.4860$.

TABLE 1: Excited-state Properties of the Two Molecules in Solution without the Metal[a]

		energy (eV)	λ (nm)	osc. st.	Γ^{rad} (s^{-1})
antra	TD	2.83	438	0.7793	1.24×10^8
	Z	2.59	478	0.9586	1.66×10^8
lissa	TD	2.81	441	0.7622	1.24×10^8
	Z	2.60	476	0.9459	1.67×10^8

[a] The results obtained with TDDFT (TD) and ZINDO (Z) methods are reported.

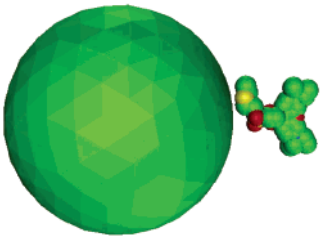

Figure 3. Representation of the cavity shape of the lissamine molecule and its orientation with respect to the metal particle. The radius of the metal particle is $R = 2.5$ nm.

3.1.2. TDDFT vs ZINDO. In this section, we present a comparison between the calculations performed at TDDFT and ZINDO levels on the systems antra and lissa, shown in parts a and b of Figure 1. The comparison regards the values of $\Gamma_{\mathrm{met}}^{\mathrm{nonrad}}$ and Γ^{rad} computed with both methods as well as the CPU time needed to perform the calculations.

Preliminary calculations on the first (four) excited states of the two molecules in solution without the metal have shown that the electronic transition of interest, which is the HOMO−LUMO ($\pi \rightarrow \pi^*$) transition, has been described at a comparable level of accuracy at both calculation levels. The values of the properties for this state are reported in Table 1.

The geometrical configuration of the systems has been chosen as reported in ref 2, thus the model molecules have been placed with the three-ring part ≃1 nm far from the metal surface. In Figure 3, the relative orientation of the lissamine with respect to the metal particle as well as the PCM cavity are shown.

Similarly to what was done in ref 11, to focus the attention on the effect of the metal particle on the studied properties, the calculated values of Γ^{rad} and $\Gamma_{\mathrm{met}}^{\mathrm{nonrad}}$ have been scaled as discussed in section 2. The values of the scaling factor f_0 are 1.256 and 1.257 for antra and lissa at the ZINDO level, respectively, and 1.694 for both the molecules at the TDDFT level.

Figures 4 and 5 show the results for $\Gamma_{\mathrm{met}}^{\mathrm{nonrad}}$ and Γ^{rad} as functions of the radius of the gold sphere for the two systems computed with the two methods. These figures clearly show

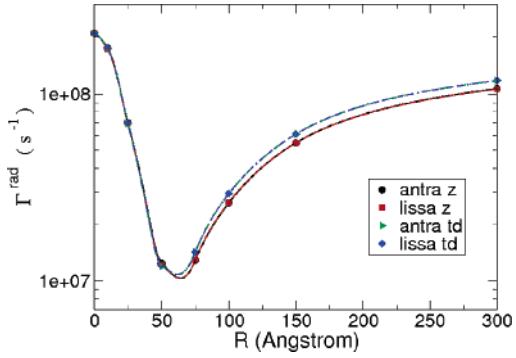

Figure 4. Radiative decay rate Γ^{rad} as a function of the metal sphere radius (R) computed at TDDFT (TD) and ZINDO (Z) levels for the systems antra and lissa. $R = 0$ indicates the system without the metal specimen.

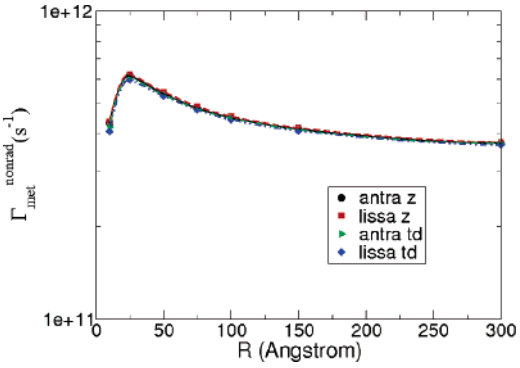

Figure 5. Nonradiative decay rate Γ_{met}^{nonrad} as a function of the metal sphere radius (R) computed at TDDFT (TD) and ZINDO (Z) levels for the systems antra and lissa. $R = 0$ indicates the system without the metal specimen.

TABLE 2: CPU Time for the Calculation of Antra and Lissa, with the Smallest and the Largest Metal Particles (R = 1 nm and R = 30 nm), Performed with TDDFT (TD) and ZINDO (Z) Methods

		CPU time (h)	
		$R = 1$ nm	$R = 30$ nm
antra	TD	17.5	18.0
	Z	1.0	1.4
lissa	TD	39.9	41.6
	Z	2.1	3.6

the good agreement between TDDFT and ZINDO results. Thus, there is no point to perform here a comparison between our ZINDO results and the experimental values, that has been already presented in ref 11 for TDDFT. For the sake of completeness, we remark that the results of Figures 4 and 5 have been obtained by correcting the metal dielectric constant for the decrease of the electron mean free path in the nanoparticle with respect to the bulk metal,[10] while the results plotted in ref 11 did not take into account such a correction (however, its effects were mentioned in the text).

Then, we report the comparison of the computational CPU time of the two methods, for the systems antra and lissa, for the smallest and the largest metal spheres ($R = 1$ nm and $R =$ 30 nm, respectively); see Table 2. The calculations have been carried out on an Amd Athlon XP 2800+.

As shown in Table 2, for the antra model, ZINDO is ≃17.5 times faster than TDDFT for the smaller sphere and ≃13 times for the larger one. For lissa, the ratios are ≃19 for the smaller sphere and ≃11.6 for the larger one. The data in Table 2 also show that the absolute time increase due to the increase of the metal sphere radius is nearly equal for TDDFT and ZINDO,

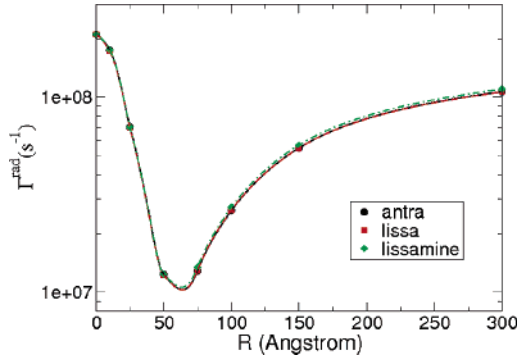

Figure 6. Radiative decay rate Γ^{rad} as a function of the metal sphere radius (R) computed at the ZINDO level for the systems antra, lissa, and lissamine with the correction for the quantum-size effect. $R = 0$ indicates the system without the metal specimen.

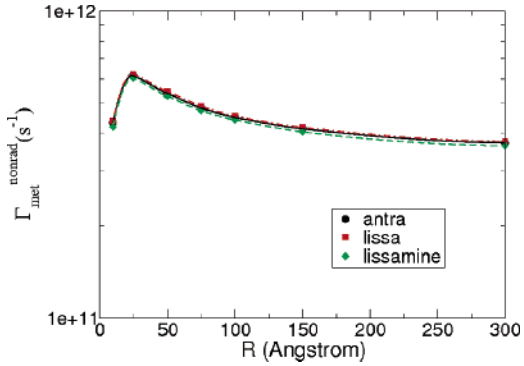

Figure 7. Nonradiative decay rate Γ_{met}^{nonrad} as a function of the metal sphere radius (R) computed at the ZINDO level for the systems antra, lissa, and lissamine with the correction for the electron limited free path. $R = 0$ indicates the system without the metal specimen.

but it is negligible with respect to the increase due to passing from antra to lissa, for which ZINDO outperforms TDDFT.

The accuracy together with the speed-up for the considered systems obtained at the semiempirical level with respect to the DFT one show the efficiency of the proposed methodology.

3.1.3. Model Systems vs Whole System. In this section, we analyze the results obtained with the simplified systems with respect to the whole lissamine (see Figure 1c). As we are now confident of the ZINDO results, we have only used this level of calculation for the three molecules. Figures 6 and 7 show the values of Γ^{rad} and Γ_{met}^{nonrad} as functions of the radius of the metal sphere. The calculations on antra, lissa, and lissamine have been performed taking into account the correction of the metal frequency-dependent permittivity for the limited mean free path of electrons, as discussed in ref 10. The scaling factor f_0 (see section 2) for the lissamine molecule is 1.214.

Both plots indicate that there is no difference in considering the whole system instead of the simplified ones. This fact demonstrates that the hypothesis proposed in ref 11 to cut the lissamine and to study just one part of that system was correct and that the main interaction between the molecule and the metal involves the three-ring aromatic part.

However, we stress the fact that with the new methodology proposed in this work, it is not necessary to cut the system under study, as these size reductions could be difficult and ineffective on other molecules. Furthermore, it is important to note that the calculations performed with ZINDO on the lissamine required a time even shorter (4.2 h for the small sphere and 8.4 h for the large one) than the ones performed with TDDFT on the most simplified molecule (antra, see Table 2).

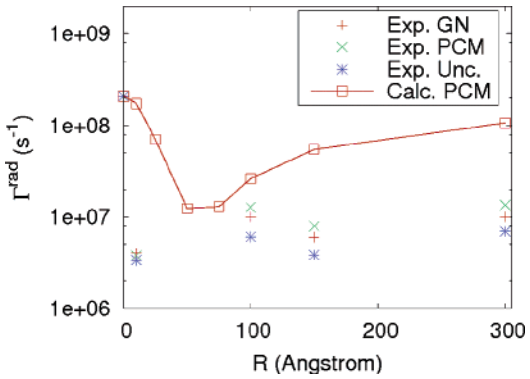

Figure 8. Radiative decay rate Γ^{rad} as a function of the metal sphere radius (R) computed at the ZINDO level for lissamine ("Calc. PCM"). The calculations have been performed with the correction for the limited electron mean free path. Experimental data are reported as given in ref 2 ("Exp. GN"), uncorrected for the absorption effects ("Exp. Unc.") and corrected for the absorption effects via PCM ("Exp. PCM"). $R = 0$ indicates the system without the metal specimen.

3.1.4. Consequences of the Absorption Process. In this last section on the lissamine molecule, we study how the experimental results are affected by taking into account the differential absorption for the molecule with the metal and without the metal. In particular, we would like to verify how large is this correction for the present case and if the discrepancy between our calculations and the experiments is reduced or amplified by the correction.

We start by considering the correction effects on the radiative lifetime. We have calculated the absorption coefficients A^{met} for the different particle radii and applied eq 4 to correct the experimental data. All the calculations have been performed by including in the metal dielectric response the effects of the limited mean electron free path, with the procedure detailed in ref 10.

In Figure 8, we report the experimental data as given in ref 2 (i.e., including the absorption correction via the GN model), the ones corrected for absorption with our model, the uncorrected experimental data, and the results of our calculations obtained with ZINDO on lissamine. When the uncorrected experimental series ("Exp. Unc.") is compared with the one corrected with PCM ("Exp. PCM"), it is evident that the magnitude of the correction can be quite large (comparable with the radiative lifetime itself). In addition, the correction changes as a function of the particle radii. The reason the corrected radiative rate is larger than the uncorrected one is that the metal reduces the molecular absorption (and thus the population of the excited state), via a mechanism of destructive interference of the molecular transition dipole and of its image in the metal. As a consequence, $I_{fluo}^{met}(t = 0)$ results to be smaller than what it should be on the basis of variation of the radiative decay only. We would also like to remark that the correction obtained by our model is quite different from that obtained with the GN approach ("Exp. GN").

Let us come to the comparison with our calculated results. It is evident that the absorption correction reduces the discrepancy among the experiments and the calculations, even if the gap remains fairly large. Remarkably, the experimental values corrected with PCM ("Exp. PCM") are the closest to our computed values ("Calc. PCM"). Here, we would like to remark on the importance of properly considering in the experimental data all the possible phenomena that may affect the measured fluorescence intensity and that can modify the intensity of the exciting light, such as the absorption (and the incoherent scattering) of the metal particles at the frequency of the incident and emitted radiations (which, however, are indeed taken into account in refs 2 and 3). Although some calculations can be done in this direction (we demonstrated in ref 11 the possibility of calculating polarizability, and thus absorption cross sections, for the metal particle alone within our model), the results also depend on the details of the experimental setup (such as the length of the optical path, the concentration of the particles, the level of monochromaticity of the incident, and emitted light).

Finally, we comment on the effects of the absorption correction on the *nonradiative* decay rate. We recall that this is obtained in experiments as the difference of the total decay rate and the radiative decay rate. Since $\Gamma^{nonrad} \gg \Gamma^{rad}$ for all the particle radii considered in ref 2, the absorption correction discussed for the radiative decay rate has no effects, in the present case, on the nonradiative one.

3.2. Cy5. *3.2.1. Computational Details.* Geometry optimizations have been performed at AM1-PCM levels, and only semiempirical (ZINDO) calculations have been performed for the optical properties. For all the calculations, the PCM cavity is built as a series of interlocking spheres centered on atoms with radii:[21] 1.7 Å for C, 1.9 Å for CH, 2.0 Å for CH_n ($n = 2$, 3), 1.52 Å for O, 1.6 Å for N, 1.8 Å for S, and 1.2 Å for H not bonded to C, all multiplied by a cavity size factor of 1.2.

As for the solvent, since the molecule is placed on top of a layer of DNA strains, in describing the dielectric environment, an additional interface between the pure solvent and organic layer should be considered. Nonetheless, since we are dealing with optical responses, the effect of the two phases on the molecular decay rates should be similar (the optical dielectric constant of a continuous medium that models DNA is given by $\epsilon_\infty = 2.0$, which is not far from the optical constant of water previously reported in section 3.1.1). As a first approximation, we decided to neglect this additional interface and to study the decay rates of the Cy5 dye both in pure water and in a pure DNA-like dielectric medium.

For the metal, gold, the values of the dielectric constants at the different frequencies have been taken from the handbook of Palik:[22] for the emission process, at 665 nm, we have used $\mathrm{Re}\{\epsilon^{met}\} = -12.223$ and $\mathrm{Im}\{\epsilon^{met}\} = 1.141$; for the absorption process, at 400 nm, we have used $\mathrm{Re}\{\epsilon^{met}\} = -1.0769$ and $\mathrm{Im}\{\epsilon^{met}\} = 6.4860$.

Calculations have been repeated for all the different experimental values of the separation between the molecule dye and the metal surface (22, 24, 28, 37, 43, 70, 83, 102, 121, and 162 Å). Since the orientation of the molecule with respect to the surface is unknown, calculations have been performed for the two extreme cases, that is, for the molecular transition dipole oriented either perpendicular or tangential to the surface. As for the nonradiative decay, in contrast to the experimental value of $\Gamma_0^{nonrad} = 5.4 \times 10^8\ s^{-1}$ for the dye in solution without the metal, the experimental asymptotic value of $\Gamma_{d\to\infty}^{nonrad} = 1.08 \times 10^9\ s^{-1}$ has been used in eq 2, to take care of the nonradiative decay processes related to the precise molecular environment in the experiments.

3.2.2. Results. The calculated radiative and nonradiative decay rates for the two orientations considered have been reported in Figures 9−11, as a function of the distance between the chromophore and the metal sphere, together with the quantum efficiency of the system.

The coincidence of the results obtained using water and a DNA-like medium as pure solvents (the latter results are not shown) supports our approximation of neglecting the interface between the two dielectric. In both solvents, the molecular orientation with the transition dipole tangential to the metal

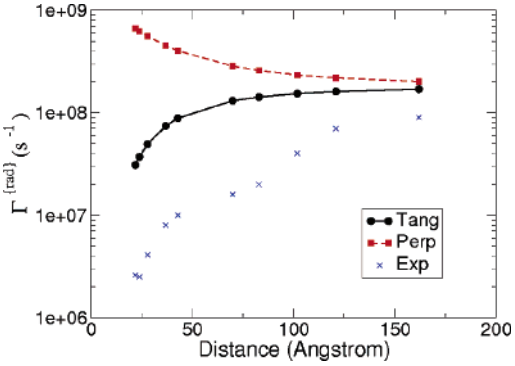

Figure 9. Radiative decay rate for Cy5 as a function of the metal−molecule distance for two different relative orientations. "Tang" refers to the molecule with the transition dipole tangential to the metal surface, and "Perp" indicates that the transition dipole is perpendicular to the metal surface. "Exp" refers to the data from ref 3.

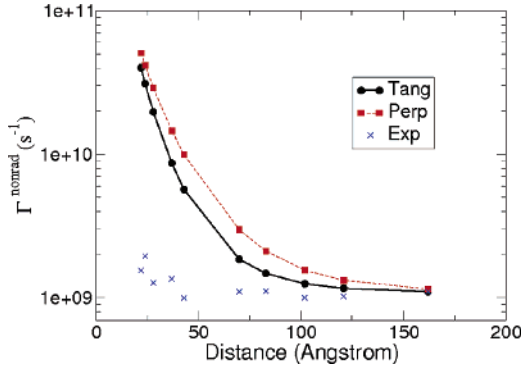

Figure 10. Nonradiative decay rate for Cy5 as a function of the metal−molecule distance for two different molecular orientations. "Tang" refers to the molecule with the transition dipole tangential to the metal surface, and "Perp" indicates that the transition dipole is perpendicular to the metal surface. "Exp" refers to the experimental data from ref 3.

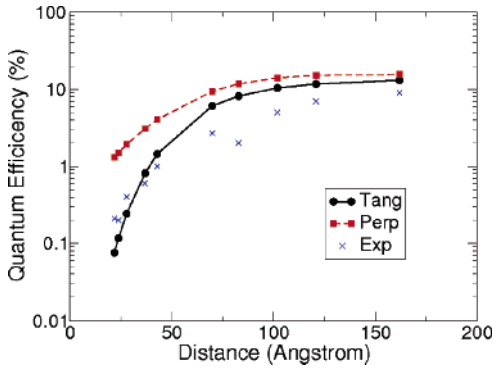

Figure 11. Quantum yield for Cy5 as a function of the metal−molecule distance for two different relative orientations. "Tang" refers to the molecule with the transition dipole tangential to the metal surface, and "Perp" indicates that the transition dipole is perpendicular to the metal surface. "Exp" refers to the data from ref 3.

surface gives results in better agreement with the experiments. Nonetheless, a significant deviation (almost 1 order of magnitude) with respect to the experimental values is present, both for the radiative and the nonradiative processes. The agreement between the calculated and the experimental quantum efficiency is due to the cancellation of the errors in the two decay rates.

Such a discrepancy is similarly present in the Gersten−Nitzan results reported in ref 3 and the considerations reported therein hold also for our results. In particular, the low experimental values of the nonradiative decay rate can be attributed to the interaction between the excited chromophore and the nearby

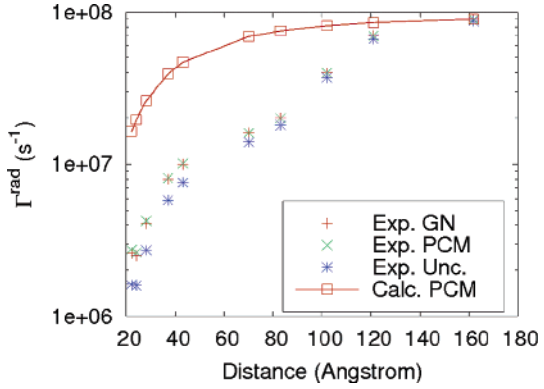

Figure 12. Radiative decay rate Γ^{rad} as a function of the metal−molecule distance computed at the ZINDO level for Cy5 ("Calc. PCM"). The calculations have been performed with the correction for the limited electron mean free path. Experimental data are reported as given in ref 3 ("Exp. GN"), uncorrected for the absorption effects ("Exp. Unc.") and corrected for the absorption effects via PCM ("Exp. PCM").

guanine basis of adjacent DNA molecules. It is worth noting that our model gives substantially the same results of the GN model, despite the fact that the two theories have quite different starting points. In the present case, the simple dipole approximation gives similar results to our QM/semiempirical description. This can be justified by considering that the molecule is always quite far from the metal surface. Nonetheless, the reported comparison is still an implicit validation of the treatment of the dielectric/metallic environment in our PCM-based model. We also remark that our model can easily handle complex-shaped metal particles and complex metal−molecule configurations, thus being of general applicability.

Finally, we would like to comment on the effects of the absorption correction, given by eq 4, on the experimental data reported for Cy5. We have applied our model to calculate the ratio A^0/A^{met} for the proper excitation frequency, as done for lissamine in section 3.1.4.

The experimental results corrected with our model are reported in Figure 12, together with the original data (corrected with the GN approach), the uncorrected experimental data, and our computed values (for the tangential orientation). The correction due to the differential absorption is smaller in this case than for the lissamine molecule, although a 70% correction is obtained for the smallest distance. This is easily understood by considering that lissamine is much closer to the metal than Cy5. However, we remark that also in this case the absorption correction reduces the discrepancy between experiment and theory. In the present case, the values corrected with our model ("Exp. PCM") and with the GN one ("Exp. GN") are very similar, as one can expect due to the large molecule−metal distance which justifies the dipole approximation.

4. Conclusions

In this article, we have presented the extension of our previously developed model to a semiempirical QM treatment of the molecular properties and the application of this method to systems that have been recently studied by optical experiments. The results have confirmed that, at least for the studied molecules, the application of ZINDO allows for the study of larger molecular dyes keeping the same level of accuracy as DFT. In addition, ZINDO is much faster than DFT (1 order of magnitude), allowing us to treat the dye molecules really used in the experiments, with an increase in the reliability of the model.

We have also demonstrated that our model not only is useful as a tool to directly calculate radiative and nonradiative rates for molecules close to metal particle but also provides quantities (such as the molecular absorption coefficient in the presence of the metal) that cannot be measured trivially (it would require to estimate the absorption coefficient of the molecule in the presence of the metal, in a spectral region where the metal absorbs as well) and that can be used to correct the experimental data themselves. In particular, we have discussed how the metal effects on the absorption can modify the experimental results. We have also seen that, for both the considered molecules, considering such an absorption correction reduced the discrepancy between calculation and experiments, although the discrepancy remains. Different reasons to explain this discrepancy have been discussed in ref 11 and in the present article, ranging from shortcomings of the model (lacks of nonlocal metal response) to possible experimental causes. Although the explanation of these discrepancy is not clear yet, we are confident that refinements of our models and of the experimental data will shed light on the important effects of the metal on the molecular de-excitation.

Acknowledgment. The authors thank Prof. Benedetta Mennucci for useful discussions and suggestions. M.C. and O. A. thank MIUR "Progetto Giovani Ricercatori" for financial support.

References and Notes

(1) Chance, R. R.; Prock, A.; Silbey, R. *Adv. Chem. Phys.* **1978**, *37*, 1.

(2) Dulkeith, E.; Morteani, A. C.; Niedereichholz, T.; Klar, T. A.; Feldmann, J.; Levi, S. A.; Van Veggel, F. C. J. M.; Reinhoudt, D. N.; Möller, M.; Gittins, D. I. *Phys. Rev. Lett.* **2002**, *89*, 203002.

(3) Dulkeith, E.; Ringler, M.; Klar, T. A.; Feldmann, J.; Muñoz Javier, A.; Parak, W. J. *Nano Lett.* **2005**, *5*, 585.

(4) Gersten, J.; Nitzan, A. *J. Chem. Phys.* **1981**, *75*, 1139.

(5) Ruppin, R. *J. Chem. Phys.* **1982**, *76*, 1681.

(6) Metiu, H. *Prog. Surf. Sci.* **1984**, *17*, 153.

(7) Ekardt, W.; Penzar, Z. *Phys. Rev. B* **1986**, *34*, 8444.

(8) Leung, P. T. *Phys. Rev. B* **1990**, *42*, 7622

(9) Kreibig, U.; Vollmer, M. *Optical Properties of Metal Clusters*; Springer-Verlag: Berlin, 1995.

(10) Corni, S.; Tomasi, J. *J. Chem. Phys.* **2001**, *114*, 3739. Corni, S.; Tomasi, J. *Chem. Phys. Lett.* **2001**, *342*, 135. Corni, S.; Tomasi, J. *J. Chem. Phys* **2002**, *116*, 1156. Corni, S.; Tomasi, J. *J. Chem. Phys* **2002**, *117*, 7266.

(11) Andreussi, O.; Corni, S.; Mennucci, B.; Tomasi, J. *J. Chem. Phys.* **2004**, *121*, 10190.

(12) Bacon, A. D.; Zerner M. C. *Theor. Chim. Acta* **1979**, *53*, 21. Correa de Mello, P.; Hehenberger, M.; Zerner, M. C. *Int. J. Quantum Chem.* **1982**, *21*, 251. Zerner, M. C. *J. Chem. Phys.* **1975**, *62*, 7, 2788. Zerner, M. C. *Reviews in Computational Chemistry*; Limpkowitz, K. B., Boyd, D. B., Eds.; VCH Publishing: New York, 1991; Vol. 2, pp 313−366.

(13) Anger, P.; Bharadwaj, P.; Novotny, L. *Phys. Rev. Lett.* **2006**, *96*, 113002.

(14) Mennucci, B.; Cammi, R.; Tomasi, J. *J. Chem. Phys.* **1998**, *109*, 2798. Cammi, R.; Mennuci, B.; Tomasi, J. *J. Chem. Phys.* **1999**, *110*, 9877. Tomasi, J.; Mennucci, B.; Cammi, R. *Chem. Rev.* **2005**, *105*, 2999.

(15) Frisch, M. J.; Trucks, G. W.; Schlegel, H. B.; Scuseria, G. E.; Robb, M. A.; Cheeseman, J. R.; Montgomery, J. A., Jr.; Vreven, T.; Kudin, K. N.; Burant, J. C.; Millam, J. M.; Iyengar, S. S.; Tomasi, J.; Barone, V.; Mennucci, B.; Cossi, M.; Scalmani, G.; Rega, N.; Petersson, G. A.; Nakatsuji, H.; Hada, M.; Ehara, M.; Toyota, K.; Fukuda, R.; Hasegawa, J.; Ishida, M.; Nakajima, T.; Honda, Y.; Kitao, O.; Nakai, H.; Klene, M.; Li, X.; Knox, J. E.; Hratchian, H. P.; Cross, J. B.; Adamo, C.; Jaramillo, J.; Gomperts, R.; Stratmann, R. E.; Yazyev, O.; Austin, A. J.; Cammi, R.; Pomelli, C.; Ochterski, J. W.; Ayala, P. Y.; Morokuma, K.; Voth, G. A.; Salvador, P.; Dannenberg, J. J.; Zakrzewski, V. G.; Dapprich, S.; Daniels, A. D.; Strain, M. C.; Farkas, O.; Malick, D. K.; Rabuck, A. D.; Raghavachari, K.; Foresman, J. B.; Ortiz, J. V.; Cui, Q.; Baboul, A. G.; Clifford, S.; Cioslowski, J.; Stefanov, B. B.; Liu, G.; Liashenko, A.; Piskorz, P.; Komaromi, I.; Martin, R. L.; Fox, D. J.; Keith, T.; Al-Laham, M. A.; Peng, C. Y.; Nanayakkara, A.; Challacombe, M.; Gill, P. M. W.; Johnson, B.; Chen, W.; Wong, M. W.; Gonzalez, C.; Pople, J. A. *Gaussian 03*, revision B.05; Gaussian, Inc.: Pittsburgh, PA, 2003.

(16) Aussenegg, F. R.; et al. *Surf. Sci.* **1987**, *189*, 935.

(17) Caricato, M.; Mennucci, B.; Tomasi, J. *J. Phys. Chem. A* **2004**, *108*, 6248.

(18) Cancès, E.; Mennucci, B.; Tomasi, J. *J. Chem. Phys.* **1997**, *107*, 3032. Cancès, E.; Mennucci, B.; Tomasi, J. *J. Phys. Chem. B* **1997**, *101*, 10506. Cancès, E.; Mennucci, B. *J. Math. Chem.* **1998**, *23*, 309.

(19) Foresman, J. B.; Head-Gordon, M.; Pople, J. A.; Frisch, M. J. *J. Phys. Chem.* **1992**, *96*, 135. McWeeny R. *Methods of Molecular Quantum Mechanics*, 2nd ed.; Academic: London, 1992.

(20) Becke, A. *J. Chem. Phys.* **1993**, *98*, 5648.

(21) Bondi, A. *J. Phys. Chem.* **1964**, *68*, 441.

(22) Palik, E. D. *Handbook of Optical Constants of Solids*; Academic: Orlando, FL, 1985; Vol. 1.